ASIA TURBOMACHINERY & PUMP SYMPOSIUM
12 - 15 MARCH 2018
SUNTEC SINGAPORE

METALLURGICAL FAILURE ANALYSIS OF STEAM TURBINE, COMPRESSOR, AND HOT GAS EXPANDER COMPONENTS

David Dowson
Service Engineer (Materials & Repairs)
Elliott Group
Jeannette, PA, USA

David Dowson is a Service Engineer with the Elliott Group, in Jeannette, Pennsylvania. He has been involved with material related failure analysis, repairs to rotating and non-rotating equipment, and aftermarket support. He has co-authored papers on materials selection for hot gas expanders, repairs to turbomachinery components, defect tolerant design concepts and remaining life assessment. Mr. Dowson received his B.S. degree (2003) from the University of Pittsburgh.

ABSTRACT

When components fail it is usually unexpected and the root cause is not always known. Downtime from failure can cost a company many thousands of dollars a day depending on the type of equipment. This cost can be magnified if the equipment failure becomes reoccurring. Identifying the root cause for a failure is paramount in preventing it from reoccurring. Components fail due to a number of reasons such as but not limited to improper design, poor material selection, off design and poor service conditions. In order to determine why a component fails one needs to perform a root cause failure analysis (RCFA). A metallurgical analysis is one of the key components of a comprehensive RCFA.

This paper will outline the stages involved when conducting a metallurgical failure analysis. Details on the techniques used and the various damage mechanisms observed on failed components will also be presented. Other analysis used to support a metallurgical examination when conducting a comprehensive RCFA will be briefly discussed. Finally, several case studies involving failure of turbomachinery components will be shown. Subjects will include high temperature corrosion on hot gas expander blades and stress corrosion cracking of steam turbine disks and compressor impellers.

INTRODUCTION

Failures of turbomachinery such as steam turbines, centrifugal compressors and hot gas expanders results in significant revenue loss every year. Costs can be magnified further if the failure becomes reoccurring due to not identifying the cause of failure. Paramount to any repair of a failed component is identifying the cause and establishing actions/procedures to prevent its reoccurrence.

Some of the tools utilized to determine a root cause include nondestructive testing, metallurgical failure analysis, mechanical property testing, stress analysis using finite element methodology, frequency and modal testing, fracture mechanics methodology, life assessment and other engineering tools as needed. This paper's primary focus will be on metallurgical analysis and steps taken to identify the cause of failure. Below shows the principle stages of a failure analysis [1].

1. Collection of background data and selection of samples
2. Preliminary examination of failed part (visual examination and record keeping)
3. Nondestructive testing
4. Mechanical testing (including hardness and toughness testing)
5. Selection, identification, preservation and/or cleaning of all specimens
6. Macroscopic examination and analysis (fracture surfaces, secondary cracks and other surface phenomena)
7. Microscopic examination and analysis
8. Selection and preparation of metallographic sections
9. Examination and analysis of metallographic sections
10. Determination of failure mechanism
11. Chemical analyses (bulk, local, surface corrosion products, deposits or coatings and microprobe analysis)
12. Analysis of fracture mechanics

13. Testing under simulated service conditions (special tests)
14. Analysis of all evidence leading to formulation of conclusions and writing the report (including recommendations).

GATHERING EVIDENCE

A failure analysis should be treated as a crime scene investigation. It is crucial that failed components and other physical evidence are gathered for analysis as soon as possible. The longer the time between failure and investigation the chance for contamination or damage of the components increases. Failed components should be stored in a clean and dry location. The broken sections should not be fitted back together as this can damage the fracture surfaces. Cleaning processes of any kind should be avoided as this removes vital evidence to the investigation. Figure 1 shows a steam turbine blade failure that was blast cleaned which severely hampered the investigation.

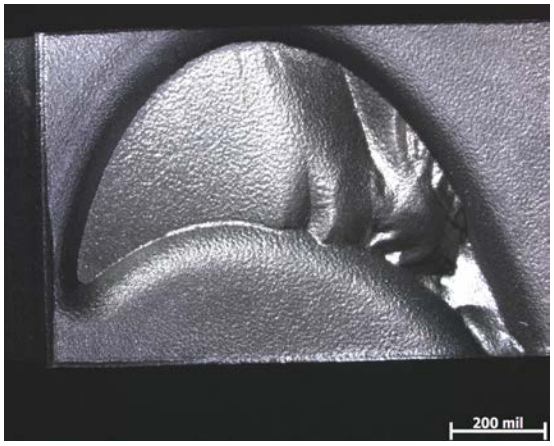

Figure 1. Blast cleaned steam turbine blade which removed all identifiable features

Photographs should be taken of the component following failure as soon as possible. In the digital age photographs are inexpensive so more is better. Vital information or evidence maybe contained in an early post failure photo. This is especially helpful to the metallurgist since they usually do not get to visit the site early post failure. Fractured components should be safely packaged and sent to a metallurgical lab for analysis. Additional evidence such as deposits and components that have not fractured should be collected for analysis as well.

Outside the scope of the metallurgist but vital to a failure investigation is a review of operating history. A qualified engineer should review provided data to determine that a unit is running at the recommended design conditions. Operating outside of design conditions can result in stresses and environmental conditions that could facilitate a failure. This type of analysis is heavily dependent on the thoroughness of the operational data provided.

METALLURGICAL EXAMINATION

Visual Examination

Upon receipt all components are visually inspected and photo documented. While not as powerful as a microscope, the naked eye can observe much larger areas for a better understanding of the overall picture. Dimensional checks should be performed to verify drawing requirements are met, if available.

Nondestructive Examination

All parts with no apparent cracks of fractures should be subjected to Nondestructive examination (NDE). Cracks that are discovered away from the main fracture can sometimes be more informative. These types of cracks usually occur due to the same damage mechanism as the main fracture and are in an earlier stage of failure. The most common NDE techniques used in conjunction with a metallurgical analysis are magnetic particle and liquid penetrant inspection. Figure 2 shows additional cracks away from the main fracture on an impeller during magnetic particle inspection.

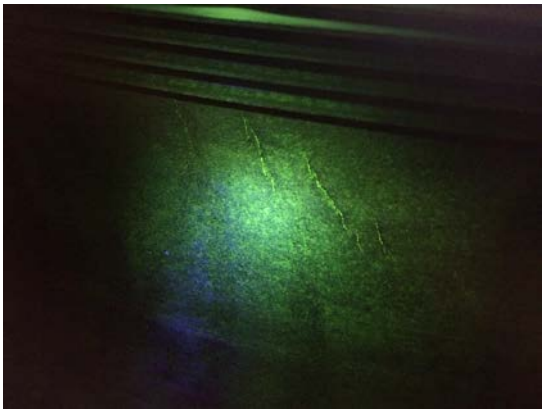

Figure 2. Cracking discovered during magnetic particle inspection of centrifugal compressor impeller

Microstructure, Mechanical and Chemical Testing

If the available material allows, failed components should undergo mechanical testing to verify the material meets design specifications. Mechanical testing usually involves tensile testing, hardness, and if necessary charpy impacts. These tests verify that the component has adequate mechanical properties for the operating conditions. Chemical testing is used to justify the components elemental constituents. This information is then compared to the material specification of the component for acceptability. A microstructural cross-section is taken to

verify the material is in the correct heat treated condition. Figure 3 shows the correct quench and tempered condition of a steam turbine blade. The main purpose of these tests is to eliminate a material issue as the cause of failure.

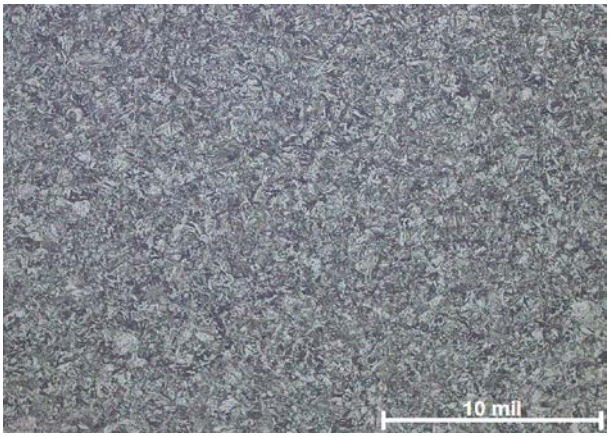

Figure 3. Quenched and tempered microstructure of AISI 403 Steam turbine blade

Failure Mechanism

Key to any metallurgical analysis is identifying the failure mechanism of the component. In turbomachinery, failures most commonly occur by one or a combination of the following mechanisms:

- Fatigue – high cycle or low cycle
- Environmentally assisted – Corrosion / Corrosion Fatigue / Stress Corrosion Cracking (SCC)
- Erosion – solid particle or liquid impingement
- Creep Rupture / Creep Fatigue
- High Temperature Corrosion/Embrittlement
- Mechanical (foreign object) Damage

The identification of the failure mechanism is accomplished by analyzing the fracture surface under stereoscopic and scanning electron microscope (SEM). Depending on the material, each failure mechanism exhibits characteristics that can be used for its identification. The following describes these mechanisms and their observed characteristics on failed turbomachinery.

Fatigue

Fatigue is the progressive localized permanent structural change that occurs in a material subjected to repeated or fluctuating strains at stresses having a maximum value less than the tensile strength of the material [1]. Therefore failures that occur under cyclic loading are termed fatigue failures. These can be vibration stresses on blades, alternating bending loads on shafts, fluctuating thermal stresses during start-stop cycles, etc. There are two types of fatigue: low cycle fatigue (LCF) and high cycle fatigue (HCF). Traditionally, low cycle fatigue failure is classified occurring below 10^4 cycles, and high cycle fatigue is above that number. An important distinction between HCF and LCF is that in HCF most of the fatigue life is spent in crack initiation, whereas in LCF most of the life is spent in crack propagation because cracks are found to initiate within three to 10 percent of the fatigue life. HCF is usually associated with lower stress, while LCF usually occurs under higher stress.

Most failures of rotating turbomachinery are due to high cycle fatigue. These failures generally occur at loads that when applied statically would produce little affect. Fatigue occurs in three stages:

I) Crack initiation
II) Crack propagation
III) Final fracture overload

Fatigue is a particularly insidious failure mechanism. A fatigue failure spends 80-90% of its life in crack initiation. This means a fatigue crack is not detectable by NDE inspection until the crack propagation stage which is the last 10-20% of its life. A component can be reaching the end of its life and yet show no physical evidence in which to identify impending failure. Typical fatigue fractures are relatively flat and smooth and in some cases show beachmarks that indicate successive positions of the advancing crack tip. Fatigue is most commonly transgranular with striations, which each one indicates a single cycle of stress. Figure 4 shows a steam turbine blade with typical high cycle fatigue fracture features.

Figure 4. High cycle fatigue failure of steam turbine airfoil

Corrosion Fatigue and Stress Corrosion Cracking

Corrosion fatigue is the combined action of repeated or fluctuating stress and a corrosive environment to produce

cracking [1]. The corrosion is typically localized and takes the form of pitting. These pits act as stress risers and when combined with an alternating stress can lead to a fatigue failure. Figure 5 shows a pit from which a fatigue crack is propagating. Corrosion fatigue can occur on both steam turbines and compressors but is more commonly seen on steam turbine blades. Figure 6 shows a steam turbine blade failure that initiated from a corrosion pit.

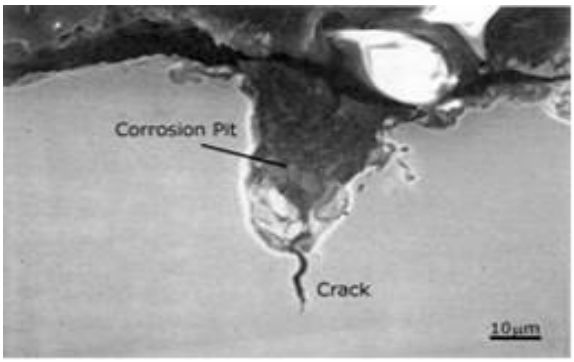

Figure 5. Fatigue crack propagating from corrosion pit

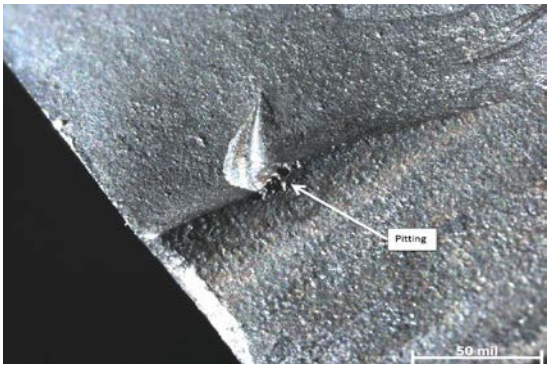

Figure 6. Corrosion pit at initiation of steam turbine blade fatigue failure

Stress Corrosion Cracking is a mechanical-environmental failure process in which sustained tensile stress and chemical attack combine to initiate and propagate fracture in a metal part [1]. Therefore in order for SCC to occur three variables are required:

1) Tensile stress
2) Corrosive environment
3) Susceptible material

Removal of any one of the above variables will prevent SCC from occurring. SCC usually initiates at stress risers such as pits due to the high peak stresses present. However, the absence of pits does not exclude the possibility the failure mechanism was SCC. SCC can be transgranular or intergranular depending on the material and the corrosion media. Cracks typically appear branched but can be straight depending on the applied stress involved. Both steam turbines and centrifugal compressors can be subjected to SCC. Unwanted carryover contaminants can lead to SCC in high stressed components such as impellers and steam turbine blades/disks. Figure 7 shows transgranular SCC of a centrifugal compressor impeller due to chlorides.

Figure 7. Transgranular SCC of impeller due to chlorides

SCC is of particular concern on last stage steam turbine disks and blades. Blades are typically manufactured from 12Cr martensitic stainless steel such as AISI 403 which can be susceptible to corrosion in a chloride environment. Chlorides such as NaCl can lead to pitting and SCC of steam turbine blades. Sodium Sulfite (Na_2SO_3) is used as an oxygen scavenger but has the potential to decompose into hydrogen sulfide. Hydrogen sulfide is a corrosive compound that can lead to sulfide stress cracking and promote hydrogen embrittlement (Figure 8).

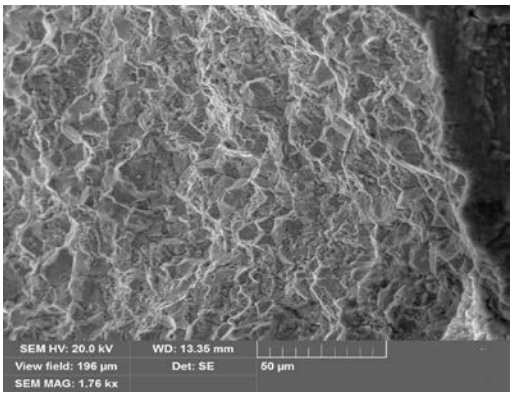

Figure 8. SEM micrograph of intergranular corrosion cracking of steam turbine blade

SCC is most commonly seen on steam turbine disk blade root attachments. The low alloy steels of steam turbine rotors are susceptible to SCC in the presence of hydroxides such as NaOH. The crack morphology of SCC on rotor materials is typically always intergranular (Figure 9).

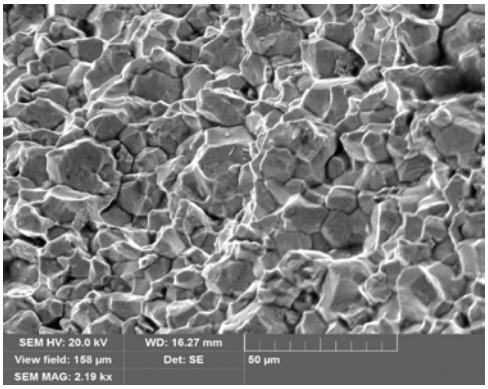

Figure 9. SEM micrograph of intergranular SCC of steam turbine disk

Erosion – Liquid or Solid Particle

Erosion is a loss of material due to mechanical interaction between the surface and liquids or particles. The liquids/particles when accelerated in steam or process gas can impact components resulting in the removal of small amounts of material. Eventually pits and microcracks form at the surface. When cyclic stresses are present the pits and microcracks will create stress concentrations from which fatigue cracks can initiate [2].

Erosion is particularly problematic for steam turbine blades. Steam turbines operate at higher temperatures and with a more closed gas path compared to centrifugal compressors. Solid particle erosion can occur on steam turbine blades due to the exfoliation of scales from piping during transient conditions (Figure 10). As the latter stages of a steam turbine increase in wetness the blades become susceptible to liquid droplet erosion. The damage typically takes the form of removal of material from the blade leading edge (Figure 11). Compressor impeller and hot gas expander blades can also experience erosion damage as well (Figures 12&13).

Figure 10. Solid particle erosion of steam turbine blades due to exfoliation of upstream piping/boiler scale

Figure 11. Liquid droplet erosion of last stage blades due to excessive moisture

Figure 12. Erosion at discharge of impeller blade

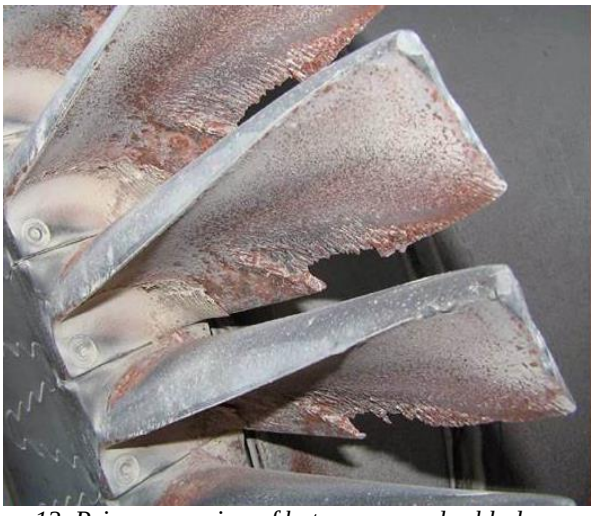

Figure 13. Primary erosion of hot gas expander blades

Creep

Creep is time dependent strain occurring under stress. After a period of time, creep may terminate in fracture by creep rupture [1]. In turbomachinery, creep is a concern on components which operate under stress at high temperatures. Evidence of creep damage in the high temperature regions of blade attachment areas of turbine rotors has been observed [3]. Creep damage takes the form of isolated then oriented cavities which link up to form cracks (Figure 14). Figure 15 shows isolated creep cavities in the weld of the nose cone strut on the inlet casing of a hot gas expander.

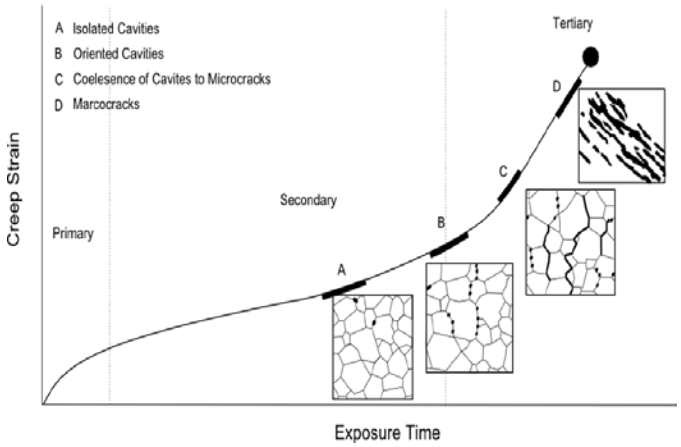

Figure 14. Stages of creep damage

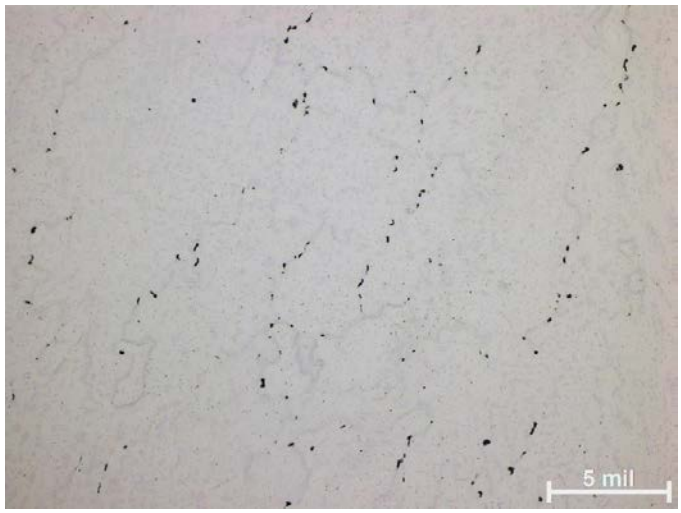

Figure 15. Oriented creep cavities in nose cone strut weld metal of expander inlet casing

High Temperature Corrosion

Fluid catalytic cracking (FCC) hot gas expanders operate in environments that can be both corrosive and erosive. Although it is well documented that the source of erosion comes from the regenerated catalyst that is carried with the hot flue gas from the FCC, its effect on high temperature corrosion is not well documented.

The nature of the corrosion attack is primarily influenced by the type of crude oil stock, which in time has a bearing on the resulting flue gas composition, regenerated catalyst and the nature and quality of additions injected into the FCC process. Blades that are subjected to partially combusted flue gas can develop oxide wedges in the root. The formation of oxide wedges plays a pivotal role in the fracture of expander blades. Oxide wedges typically occur in the upper root land on the high pressure side of the blade (Figure 16). Oxide wedge formation is a form of oxidation/sulfidation damage related to the repeated crack nucleation and growth of the corrosion layer at the oxide wedge tip. Eventually the oxide wedge grows to a critical size from which a fatigue crack can initiate. Papers published by Dowson Rishel and Stinner outline the relationship of stress and temperature on the high temperature corrosion/fracture mechanics of Waspaloy in various catalyst environments[4][5].

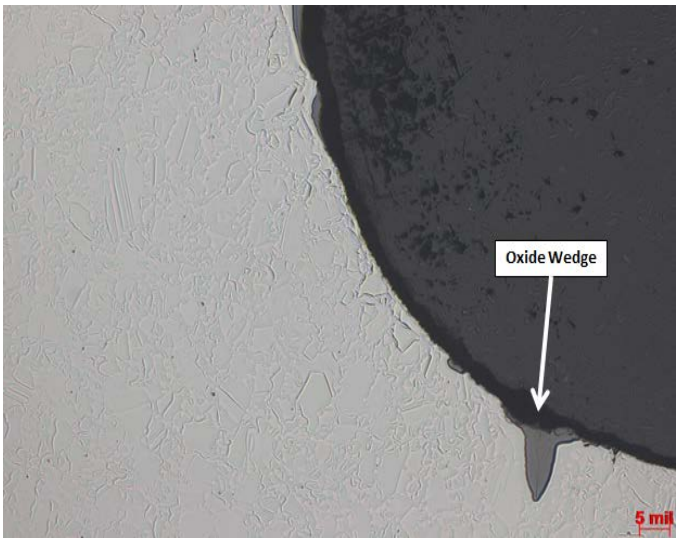

Figure 16. Cross-section of expander blade indicating the presence of an oxide wedge in the root

Mechanical Damage

Mechanical damage is caused by foreign objects that have entered the gas/steam path. Foreign objects in the gas/steam path will eventually come into contact with rotating components. The resulting impacts can exceed the yield strength of a material and cause an overload failure (Figure 17). However, typically the damage from these impacts does not directly result in failure but weakens the material which eventually leads to a fatigue failure.

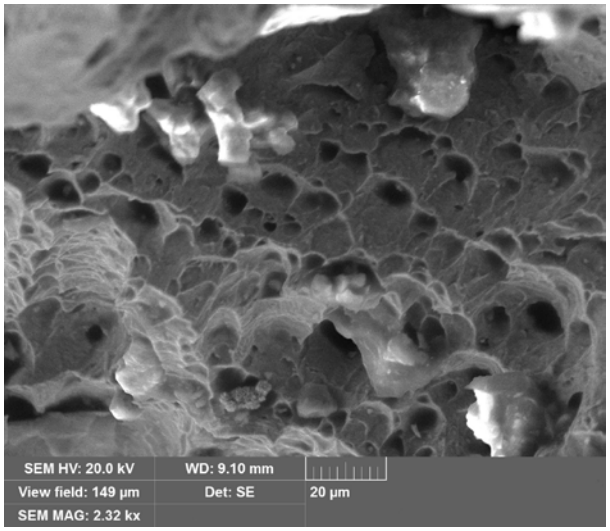

Figure 17. SEM micrograph of steam turbine blade overload failure due to foreign object impact

REPORT CONCLUSIONS

Determining the mode of failure is only the initial phase in the failure analysis. To get to the root cause of the failure a rigorous evaluation of the information is required with input from design engineers, materials engineers and process engineers etc. It is not enough to determine the mode of failure only. Why a component failed by a certain mechanism is the goal of any failure analysis. The evidence to determine a conclusive root cause can be contained in the failed components themselves. In these cases a metallurgical analysis is all that is necessary to bring a failure analysis to its final conclusions. However, as mentioned previously further analysis involving finite element analysis, modal and frequency testing, fracture mechanics etc. are necessary to provide supporting evidence for a conclusive root cause.

CASE STUDY 1

Introduction

Hot gas expander rotor experienced a single blade failure resulting in unit shutdown. The operating time of this rotor was approximately 54,000 hours. The request was made for a metallurgical failure analysis of the failed rotor.

Metallurgical Examination

Visual Examination

Initial inspection of the failed rotor indicated a single blade failure at the top fir-tree radius in the blade root section (Figure 18). All the blades were numbered in the clockwise direction on the inlet face prior to disassembly starting at failed blade #1. The blades were packaged and sent for metallurgical examination.

Figure 18. Failed blade fracture surface prior to disassembly

The blades were Non-Destructive Examined (NDE) by fluorescent penetrant and no indications were observed. There was evidence of heavy rubbing on the blade tips of all the blades due to catalyst building up on the shroud (Figure 19).

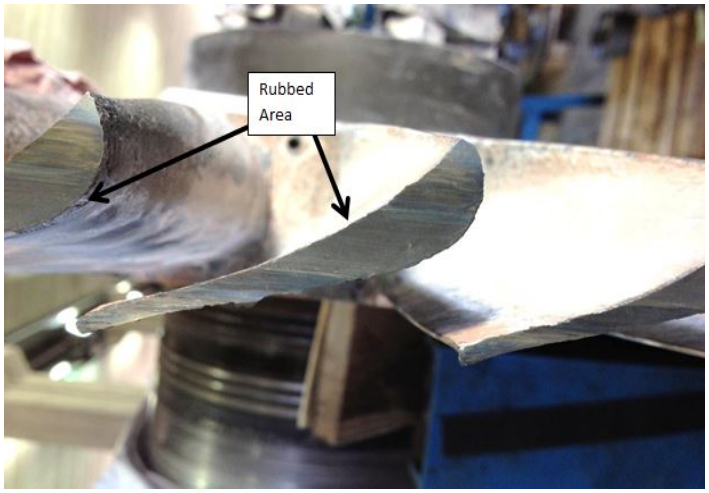

Figure 19. Blade rubbing on the airfoil tips

Chemical and Mechanical Testing

Several blades were sectioned for chemical and mechanical testing. The chemical properties of the blade material were within material specifications for Waspaloy. The mechanical test at 1000°F met the requirements for tensile and yield strength. The hardness value conformed to the requirements of Waspaloy material.

Fracture Analysis

Optical Examination

The appearance of the fracture surface of blade #1 is shown in Figure 20. The failure appeared to have initiated midway at the top fir-tree radius on the pressure side of the blade root section. Examination of the fracture surface indicated after initiating the crack propagated through the blade until overload failure at the discharge side of the blade. Located at the point of initiation were flat and smooth areas which are explained in more detail in the Scanning Electron Microscope (SEM) section (Figure 21). These flat and smooth areas were apparent over the crack surface inboard from the top fir tree radius. The fracture surface immediately after the flat and smooth areas had a rough appearance shown at high magnification in Figure 22.

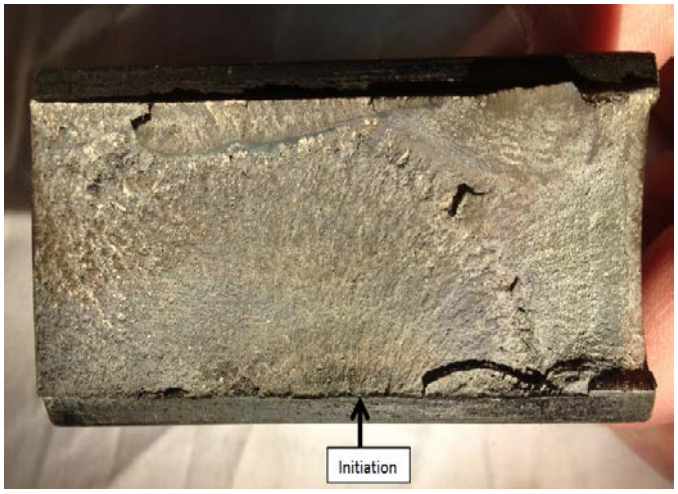

Figure 20. Fracture surface of failed blade

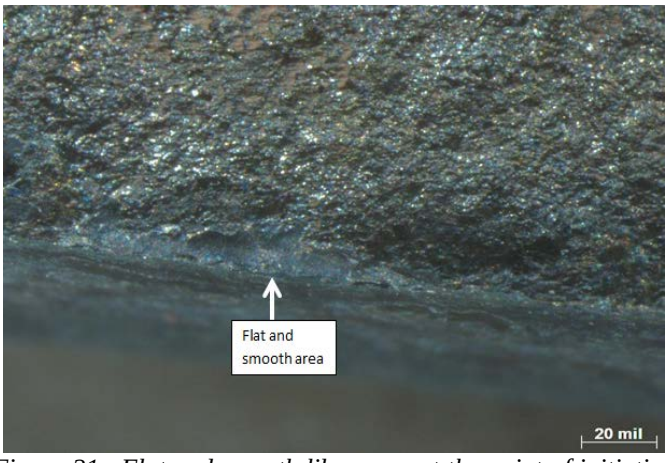

Figure 21. Flat and smooth like areas at the point of initiation inboard from the top fir-tree radius

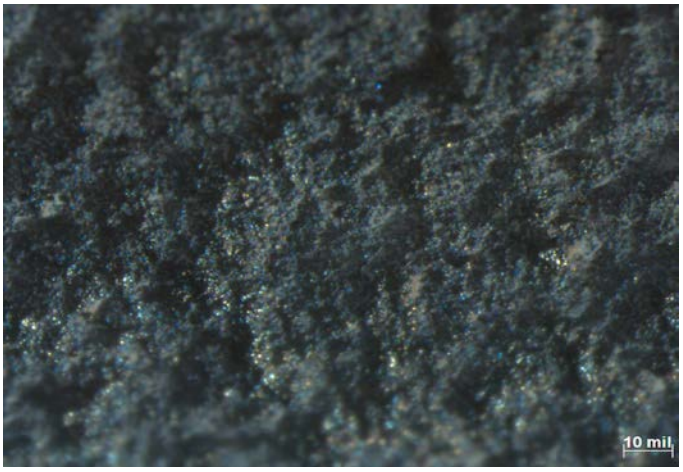

Figure 22. Initiation area at high magnification showing a rough surface appearance

SEM Examination

The flat and smooth areas at the initiation which were identified optically showed a brittle appearance when examined under the SEM. Figure 23 showing the area of deepest penetration, which was 17.11 mils. These areas of deep penetration were observed at approximately 1.25 inches from the discharge side. Energy Dispersive Spectroscopy (EDS) analysis of these areas at the initiation showed the major elements present to be Chromium, Oxygen and Sulfur (Figure 24). This indicated the areas were composed of Chromium Oxide and Chromium Sulfide. X-Ray mapping verified that this area consisted of Chromium Oxide and Chromium Sulfide (Figure 25). Note the reduction of Nickel on this area compared to the rest of the fracture surface.

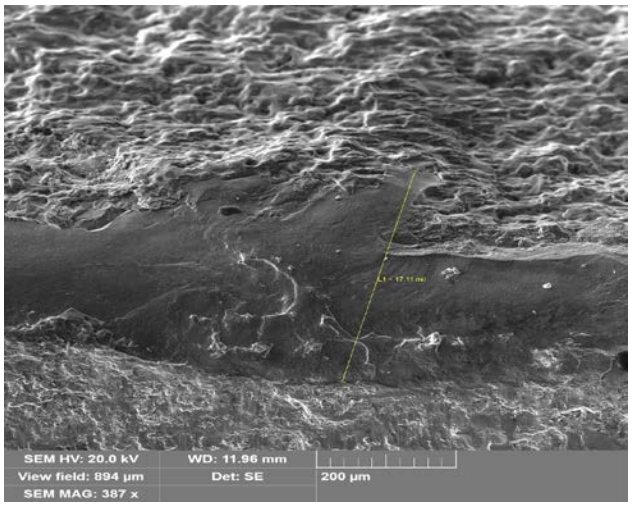

Figure 23. Flat and smooth area examined under SEM

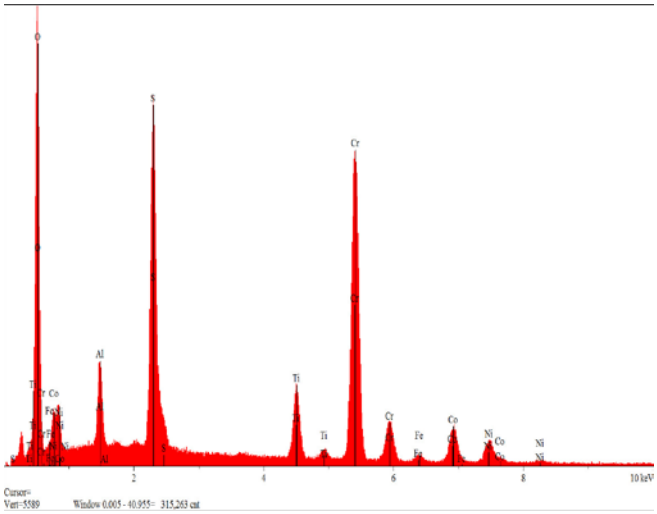

Figure 24. EDS analysis indicating the presence of Chromium Oxide and Chromium Sulfide

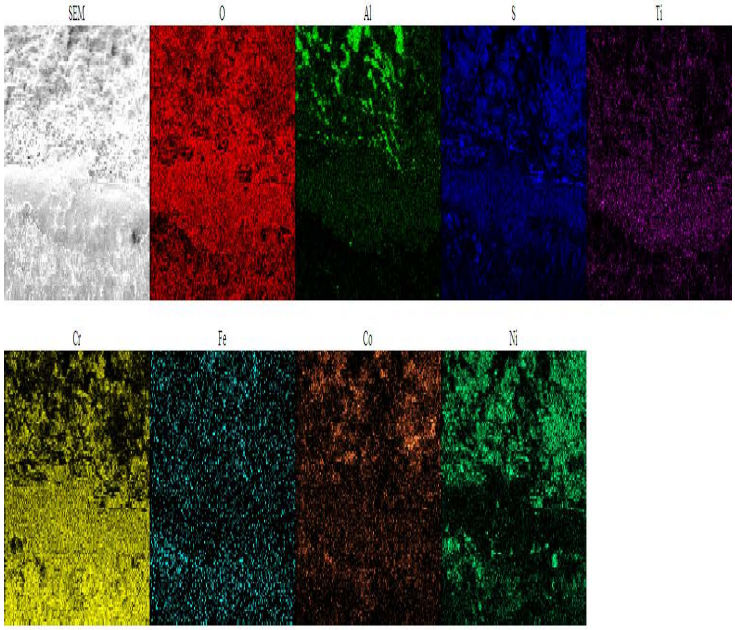

Figure 25. X-ray mapping of area in Figure 23 showing the concentration of the elements. Note the lack of Nickel (Green) in at this area.

After stripping using acetate tape some small intergranular areas could be seen near the initiation point (Figure 26). Further away from the point of initiation in which the surface is less obscured the crack propagation had an intergranular appearance (Figure 27). The crack propagated in an intergranular manner through most of the blade until final overload which showed dimple rupture (Figure 28). Final overload occurred near the discharge side on the non-pressure side of the blade.

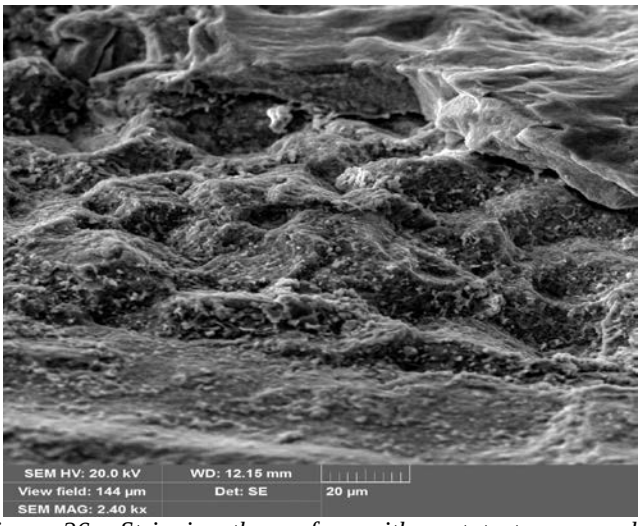

Figure 26. Stripping the surface with acetate tape revealed intergranular features

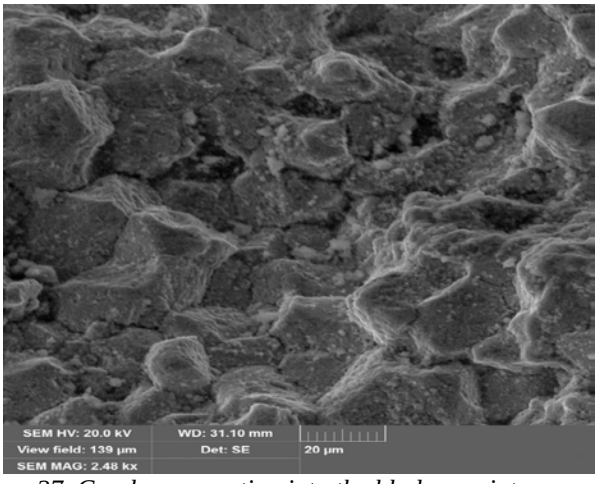

Figure 27. Crack propagation into the blade was intergranular

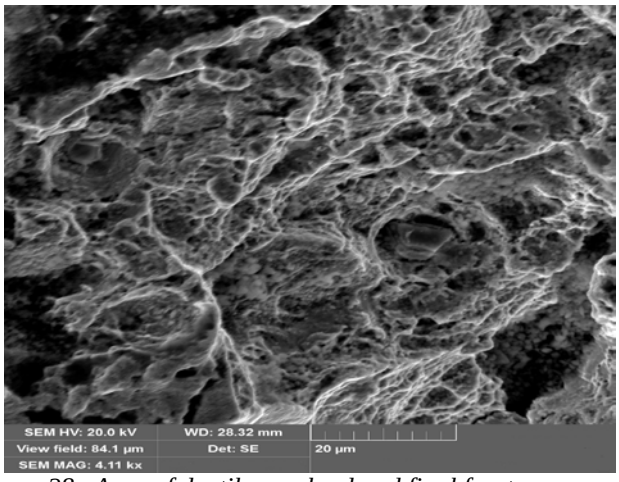

Figure 28. Area of ductile overload and final fracture

Intact Blade Cross Sections

Several blades were cross-sectioned through the root to determine if the remaining blades exhibited the same Oxide/Sulfide attack as seen on the failed blade. The manner in which the blades were cross-sectioned is shown in Figure 29.

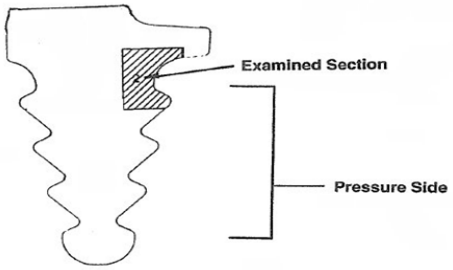

Figure 29. Area of blade cross sections

The cross-sections of blades approximately 1.25 inches from the discharge side showed evidence of oxide wedges. An oxide wedge can clearly be seen at the top root radius on the pressure side of the blade (Figure 30). High magnification of the oxide wedge revealed its length to be 11.64 mils. X-Ray mapping of the oxide wedge indicated the presence of the same elements as seen on the flat and smooth areas at the initiation of the failed blade. The oxide wedge mainly consisted of Chromium, Oxygen and Sulfur which suggest Chromium Oxide and Chromium Sulfide. In the center of the wedge was a vein rich in Nickel and Sulfur (Figure 31). Figures 32 & 33 show oxide wedges on other blades approximately 1.25 inches from the discharge side. The largest oxide wedge of 16.84 mils was found in a blade which was two blades away from the one that failed. A SEM micrograph of a cross-section of another blade revealed two oxide wedges in their infancy (Figure 34). Figure 34 illustrates how as the oxide cracks it exposes the base metal to the corrosive environment promoting deeper growth of the oxide wedges.

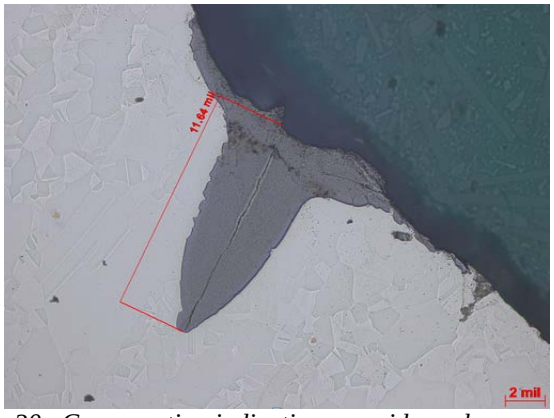

Figure 30. Cross-section indicating an oxide wedge

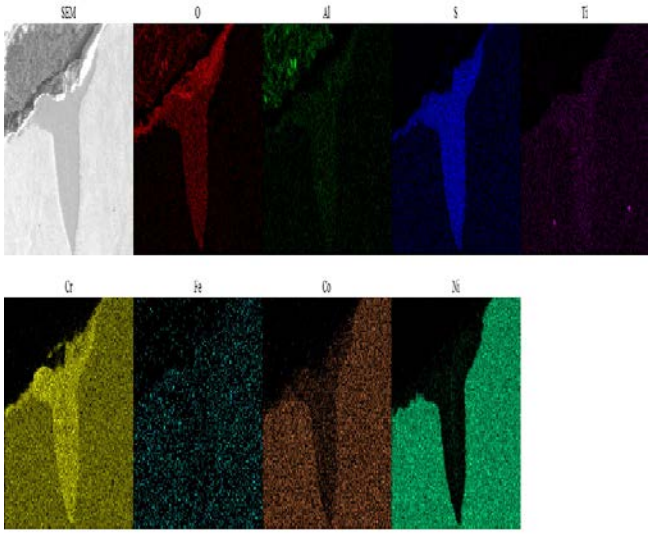

Figure 31. X-ray mapping of the oxide wedge

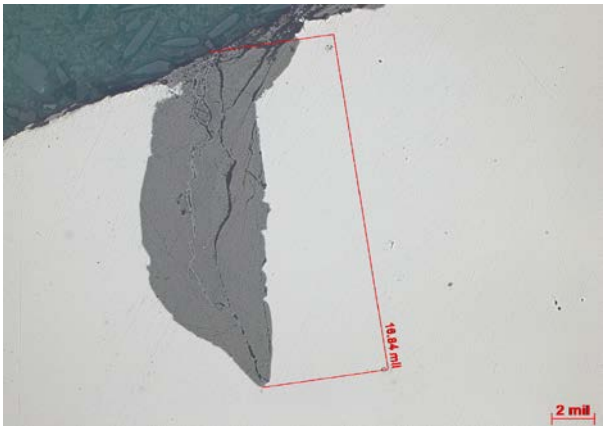

Figure 32. Oxide wedge found on a non-failed blade at 1.25" from the discharge side of the root

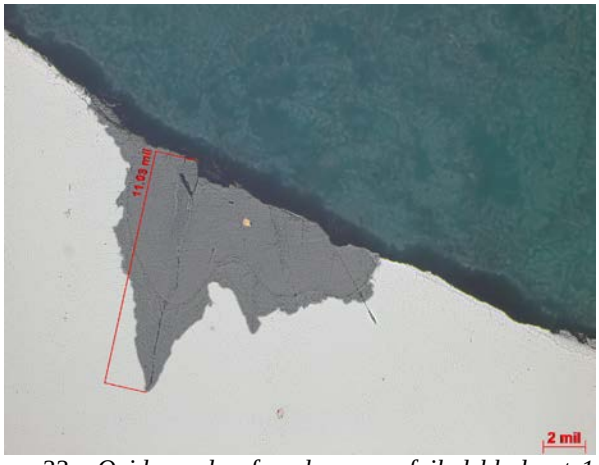

Figure 33. Oxide wedge found on non-failed blade at 1.25" from the discharge side of the root

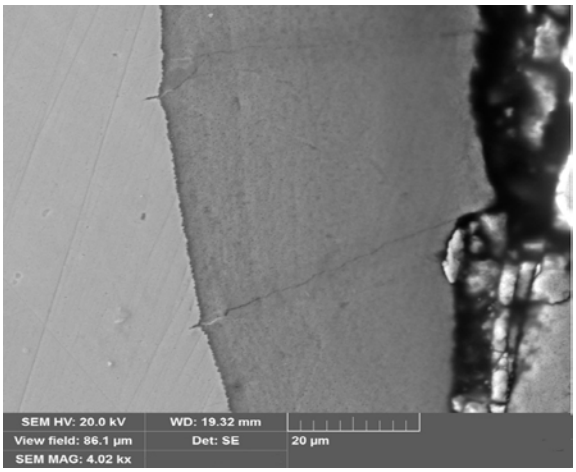

Figure 34. Early stage of oxide wedges

Discussion and Conclusion

The failure of the blade was due to corrosion fatigue that initiated at the top fir-tree radius on the pressure side. Initiation occurred due to high temperature corrosion attack and penetration indicating a corrosion assisted process. Sulfur can embrittle Nickel based superalloys as it penetrates down the grain boundaries. The intergranular propagation of the crack along the fracture surface supports a corrosion fatigue damage mechanism. The corrosion media in this case is obviously Sulfur. No material deficiency was found that could have initiated the failure.

Cross-sections of the top fir-tree radius of several intact blades showed evidence of oxide wedges. The size and depth of the oxide wedges varied along the blade with the largest being located approximately 1.25 inches from the discharge side. The point of initiation of the failed blade is approximately 1.25 inches. Oxide wedges form due to repeated crack nucleation and growth of the oxide layer at the oxide wedge tip. The rupture of the oxide at the wedge tip exposes the base metal to the corrosive environment which promotes further growth. These oxide wedges would have given rise to a significant stress concentration. It is this stress riser that initiates the crack and it is the continuing diffusion of the Sulfur into the base metal that propagates the crack under a corrosion fatigue mechanism.

The rubbing of the blade tips is a major contributor to the failure and should not be overlooked. The formation of oxide wedges is a function of the temperature, environment and stress. It has been observed during experimental testing and from past failures that an increase in the stress magnitude, whether static or dynamic, in a hot corrosive environment can result in sharp oxide wedges. The application of dynamic stresses compared to static stresses of the same magnitude tends to increase the penetration of the oxide wedges. The rubbing of the blade tips caused fretting at the contact points that contributed to the breakdown of the protected diffusion coating. The chromized coating applied to the blades should have protected this form of corrosive attack. However, the repeated rubbing of the blades against the catalyst resulted in a dynamic stress being applied in the blade roots. This dynamic stress diminished the effectiveness of the coating exposing the virgin Waspaloy material to hot corrosive attack. Since catalyst buildup on the shroud is a major contributor to the blade tips rubbing, every effort should be made to minimize the rubbing. Application of walnut shells and/or thermal cycling of the hot gas expander can assist in removing catalyst buildup before any future blade rubs occur, with minimal operating interruptions.

Due to the results of this metallurgical analysis, replacement of the disk as well as the blades was recommended. The stresses at the top fir-tree radius of the disk and blade root are very similar. This top fir-tree radius of the disk would have been exposed to the same operating temperature that promoted the formation of oxide wedges in the blade roots. Therefore, it was reasonable to assume that the disk would have experienced the same high temperature corrosion attack that occurred on the blades. Application of current NDE penetrant technologies cannot detect these oxide wedges due to the indications being filled with corrosive oxide deposits.

CASE STUDY 2

Background

The subject steam turbine experienced a 4th stage disk rim failure near the locking pin location (Figure 35). The subject steam turbine was made from Chromium-Nickel-Molybdenum-Vanadium alloy steel, ASTM A470 Grade C Class 7. The rim was parted from the main body of the disk and sent for metallurgical analysis.

Figure 35. As received condition of the 4th stage failure

Metallurgical Examination

The fracture surface of the disk rim was carefully examined and it appeared at first glance to be a fatigue failure. However, upon further examination it was determined that stress corrosion cracking (SCC) was the actual failure mechanism. The details of this analysis are summarized in the following.

Visual examination revealed additional cracking on the disk rim other than the main fracture. The additional cracks were cross-sectioned and polished. Evidence of cracking was observed initiating from three of the four fir-tree root radii. Examination under a high powered microscope indicated the cracks were intergranular and initiated from corrosion pits (Figure 36).

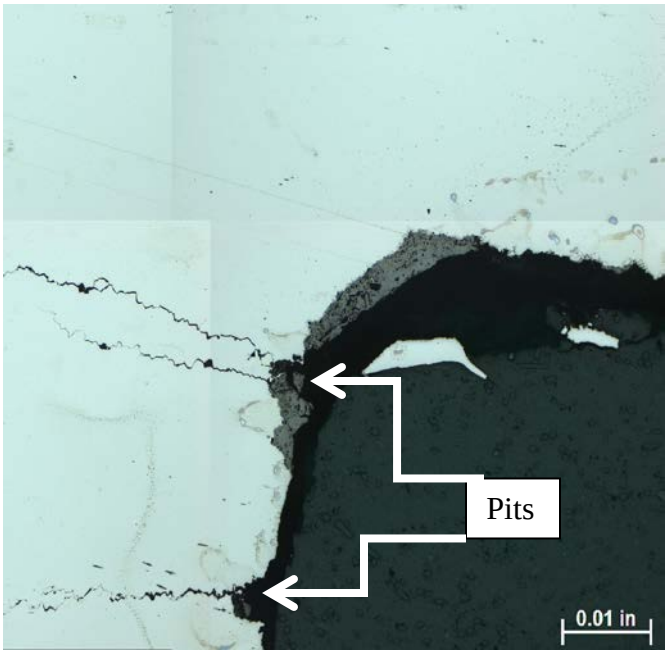

Figure 36. Corrosion pits from which the SCC initiated

Microstructure examination of the cracked disk rim area presented evidence of two different microstructures (Figure 37). Area A consisted of a fine grained untempered martensitic structure with a hardness of 42 HRC (Figure 38). This value of 42 HRC represents a significant increase in hardness compared to ASTM A470 Grade C Class 7 rotor forging specifications. Area B consists of tempered martensite and bainitic microstructure with a hardness of 26 HRC (Figure 39). Area B is more typical of an ASTM A470 Grade C Class 7 rotor forging. A cross-section of the disk rim with no evidence of cracking is shown in Figure 40. The entire cross-section exhibited a tempered martensite and bainitic microstructure with a hardness of 26 HRC (Figure 41).

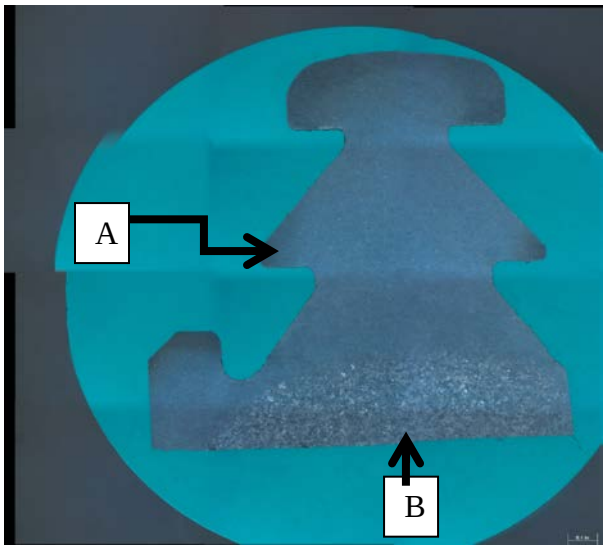

Figure 37. Two different microstructures after etching

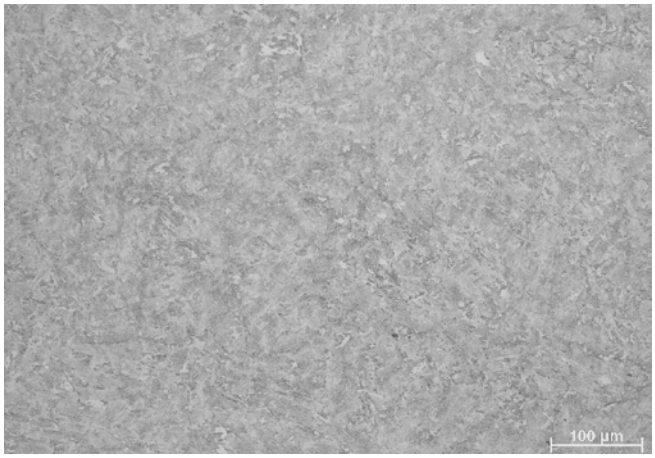

Figure 38. Fine grained untempered microstructure of area A

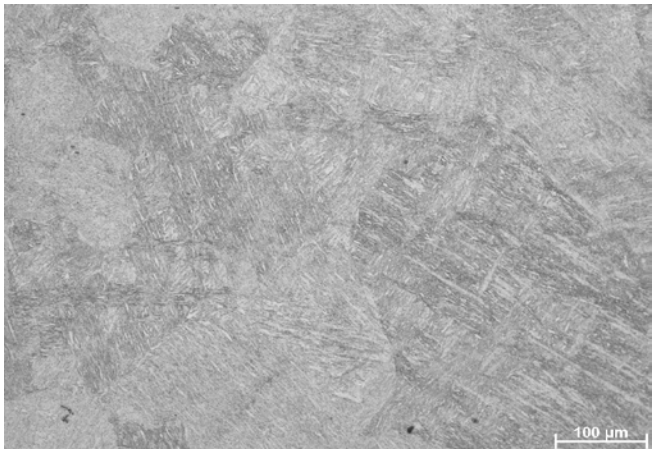

Figure 39. Tempered martensitic and bainitic microstructure of area B

Figure 40. Cross-section near the fracture with no cracks

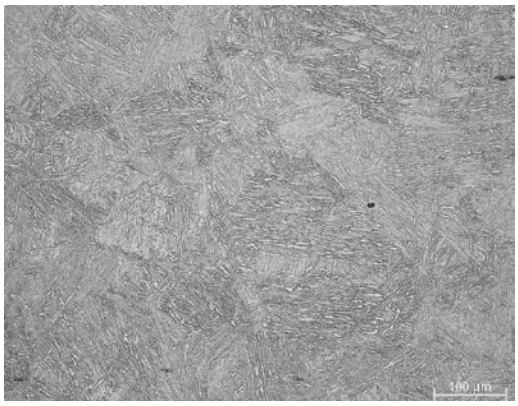

Figure 41. Cross-section in Figure 40 consists of a martensitic and bainitic microstructure

The fracture surface was examined in detail using a scanning electron microscope (SEM). All locations exhibited the same intergranular fracture surface features which is typical of SCC on steam turbine rotor material (Figures 42).

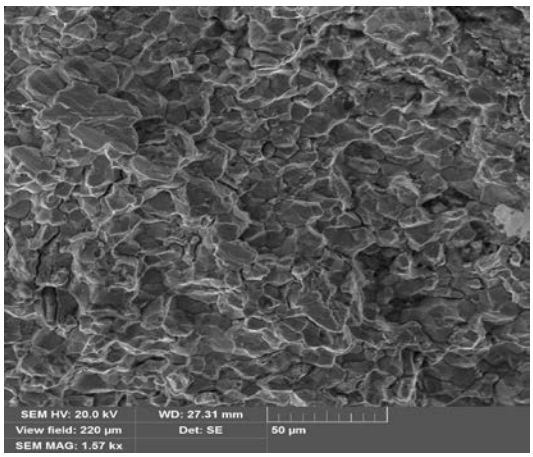

Figure 42. SEM micrograph showing typical intergranular features of SCC

Energy dispersion spectroscopy (EDS) of the corrosion pits revealed evidence of chemical contaminants. Elements such as K, S, Cl and Na were found and are well known to cause SCC (Figure 43). EDS and chemical analysis indicated the disk rim material was from an ASTM A470 Grade C Class 7 rotor forging.

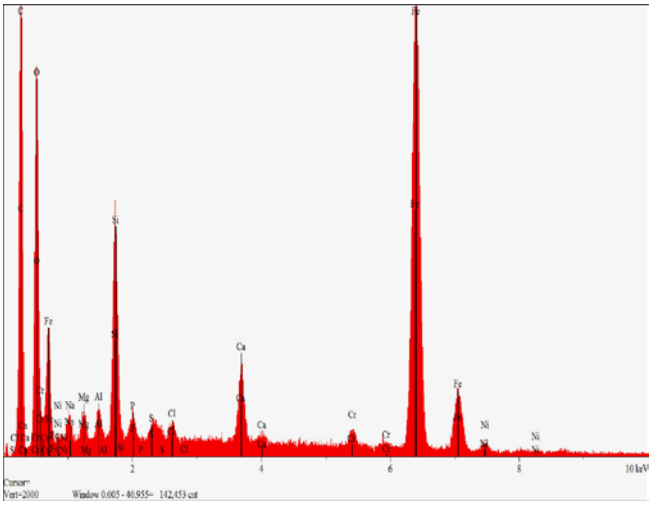

Figure 43. EDS analysis of corrosion pit indicating the presence of chemical contaminants.

Discussion and Conclusion

The failure mechanism of the subject disk rim was SCC. The chemistry of the disk rim complied with ASTM A470 Grade C Class 7 material requirements. However, there was a significant difference in microstructure and hardness between the areas of the rim with SCC and the areas without SCC. SCC only occurred in the areas with the high hardness. The cause of the SCC failure was due to a combination of high hardness material and corrosive chemical contaminants. The high hardness in the locking pin area of the disk rim would have made the material more susceptible to SCC.

The most likely cause of the high hardness is the application of high temperature to this area. If the material was heated to a temperature over its Ac_1 temperature then it would harden upon cooling. Ac_1 is the temperature in which austenite begins to form upon heating which depending on the cooling rate can form hard phases such as untempered martensite. If not followed by a tempering heat treatment then this hardness would remain high. How and when this area experienced this high temperature is unknown. However, the localized area of the high hardness and the fact the blades obscure the disk rim suggests it is unlikely the high hardness is the result of a rub during service.

It is unlikely the disk rim would have failed without the high hardness of the material and therefore a weld repair of the disk rim is recommended. The hardness value of the weld

repaired disk rim after post weld heat treatment will be significantly less than 42 HRC. Therefore, the risk of failure by SCC will be significantly reduced. It is also recommended, if possible, that an effort be made to reduce the chemical contaminants in the steam. While not the sole cause of failure, the contaminants were a contributing factor.

CASE STUDY 3

Background

The subject three stage compressor was shut down due to high vibration. During disassembly of the compressor it was observed that a section of the first stage impeller cover at the eye seal area was missing (Figure 44). A heavy deposit was observed in the gas path of all three impellers (Figure 45). The deposits were removed from all three impellers and bagged for future analysis.

Figure 44. Fractured impeller on the rotor

Figure 45. Heavy deposits observed in the gas path

Metallurgical Examination

Visual Examination

Visual examination revealed additional cracking near the eye seal area of the impeller (Figure 46). Heavy hard deposits were observed at the blade to cover transition radius (Figure 47). The heavy hard deposits appear to coincide with the location of the cracking on the cover.

Figure 46. Additional cracks observed near the eye seal area

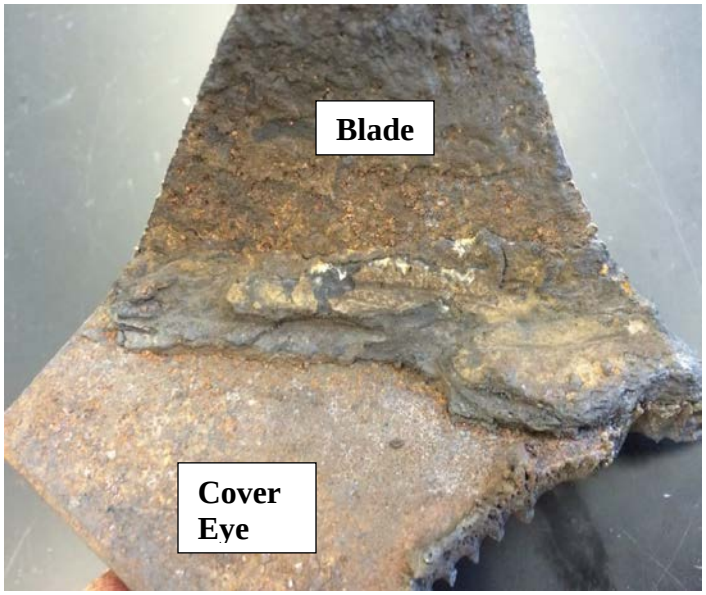

Figure 47. Heavy and hard deposits observed at the blade to cover transition radius

After visual examination the impeller was magnetic particle inspected for additional cracking. During magnetic particle inspection it was observed that the majority of the cover eye seal area had crack indications near the blade to cover transition locations.

Deposit Analysis

Deposits collected from the first, second and third stages were analyzed in the scanning electron microscope (SEM) to determine its constituent elements. Energy dispersive spectroscopy (EDS) analysis of the deposits revealed the presence of Sodium(Na), Magnesium(Mg), Aluminium(Al), Silicon(Si), Sulfur(S), Chlorine(Cl), and Potassium(K) (Figure 48). Deposits on the fracture surface of the first stage impeller revealed the presence of the same corrosive constituents.

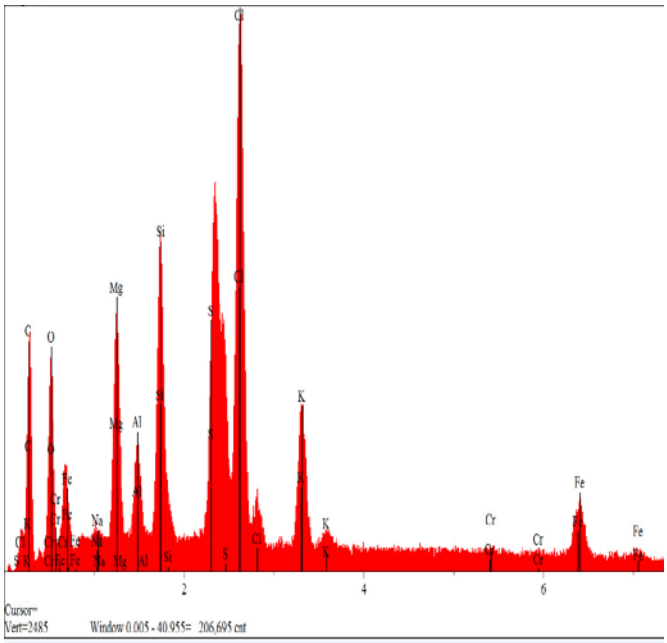

Figure 48. EDS analysis deposit presenting evidence of corrosive contaminants

Cover Crack Analysis

Cross-sections were taken through the cracks on the cover near the eye seal area (Figure 49). The initiation of the cracks occurs inside the gas path and propagates towards the outside surface. Observations after polishing indicated the presence of multiple pits inside the gas path of the cover (Figure 50). The cracks all initiated at pits such as shown in Figure 51. Further observation of the cracks revealed significant branching which is an indication of environmental corrosive attack (Figure 52). Electrolytic etching the samples verified that the cracking was transgranular morphology (Figure 53).

Figure 49. Cross-sections showing cracks initiate inside the gas path and propagate towards the outside surface

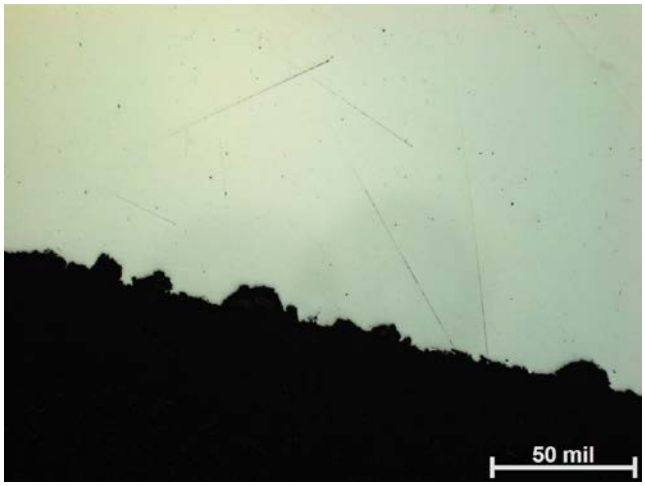

Figure 50. Multiple pits observed inside the gas path of the cover

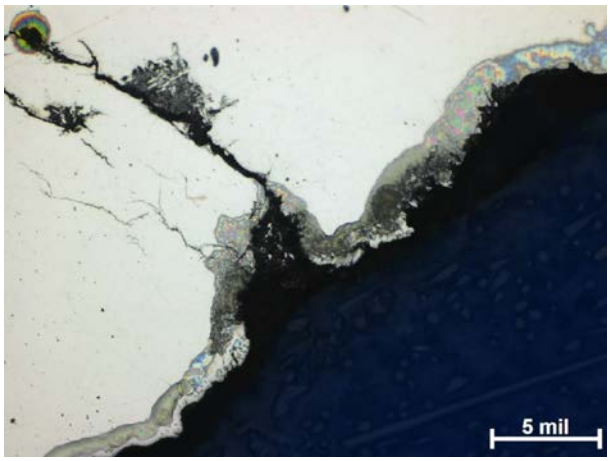

Figure 51. Initiation of the cracks occurred at corrosion pits

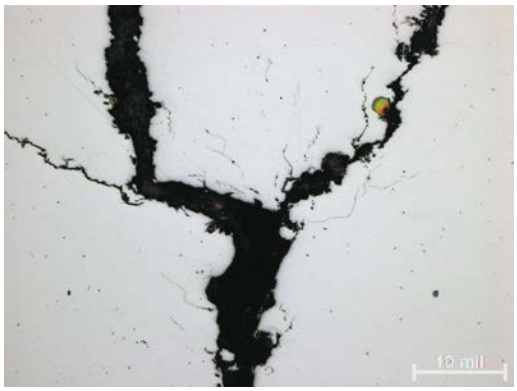

Figure 52. Significant branching was observed which is a indication of corrosive attack

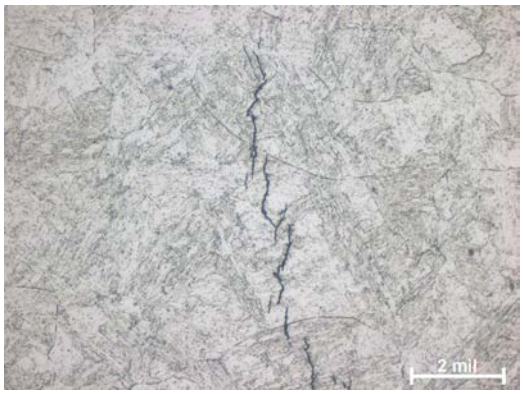

Figure 53. Transgranular morphology during crack propagation

The cross-sections were examined in the SEM using X-ray mapping to determine the corrosion contaminants inside the cracks. Observations of smaller tighter cracks that had not opened up indicated the presence of chlorides (Figure 54). This indicates that the cracking is most likely due to chlorides

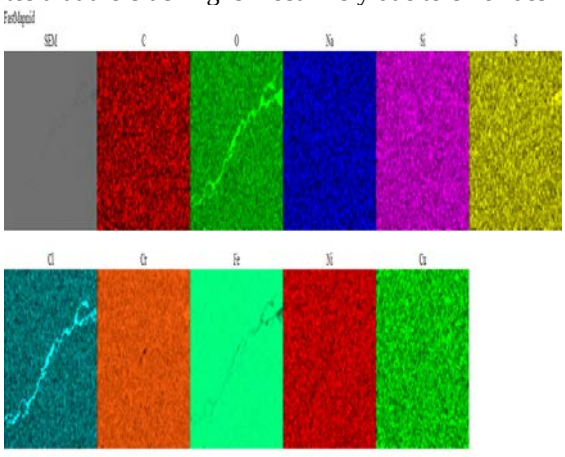

Figure 54. Smaller tighter cracks indicated the presence of chlorides(Cl) (Light Blue)

Microstructure, Hardness and Chemistry

The microstructure of the impeller material consisted of tempered martensite. Chemical analysis of the impeller indicated the material was a 15-5PH stainless steel. The microstructure, hardness and chemistry of the impeller material were within Specifications.

Discussion and Conclusions

The failure of the first stage impeller was by stress corrosion cracking (SCC) due to the presence of chlorides. The stress corrosion cracking was observed at the eye seal area near the cover to blade transition radius. The cracks initiate inside the gas path of the cover and propagated towards the outside surface. All materials were verified to be within specifications and there was no evidence that the cause of failure was due to a material deficiency.

The heavy deposits found on the rotor may have contributed to the failure. The cover to blade transition radius is one of the highest stressed locations on the impeller. The failure could have occurred due to the presence of the chloride environment combined with a high tensile stress. However, the deposits may have resulted in extremely low amounts of oxygen for the stainless steel to form its protective oxide. This will result in a localized form of attack called crevice corrosion. This would have resulted in the pits which would have compounded the crevice corrosion and allowed for the initiation of SCC. Silica can create hard deposits that will not wash off and large amounts of silicon were found during EDS analysis.

Precipitation hardened stainless steel such as 15-5PH, which the first stage was manufactured can be subject to pitting, crevice corrosion, and SCC in chloride containing environments. If it is not possible to remove the contaminants from the process gas then it may be advisable to change the impeller to a material more resistant to chlorides. Age hardened Inconel alloy 725 has superior resistance to SCC in a chloride environment compared to precipitation hardened stainless steel. A more corrosion resistant material would be a directional improvement. However, the ultimate solution is to remove the contaminants from the process gas.

CONCLUSIONS

A review of the various stages of a metallurgical failure analysis has been presented. Also presented are several case studies illustrating the application of the techniques involved. By conducting a failure analysis one can identify a root cause for fractured components and implement procedures to prevent their reoccurrence.

REFERENCES

1. Metals Handbook, Vol. 10, "Failure Analysis and Prevention," published by the American Society for Metals, Metals Park, Ohio 44073, 8th Edition, 1975
2. Dowson, P., Bauer, D. and Laney, S. 2008"Selection of Materials and Material Related Processes for Centrifugal Compressors and Steam Turbines in the Oil and Petrochemical Industry," Proceedings of the 37th Turbomachinery Symposium.
3. Bush, S.H., 1982, "Failures in Large Steam Turbine Rotors, in Rotor Forgings for Turbines and Generators," R.I. Jaffe, Ed., Pergamon Press, New York, p. I-1 to I-27.
4. Dowson, P. and Rishel, D., 1995, "Factor and Preventive Measures Relative to the High Temperature Corrosion of Blade/Disk Components in FCC Power Recovery Turbines," Proceedings of the 24th Turbomachinery Symposium.
5. Dowson, P. and Stinner, C., 2000, "The Relationship of Stress and Temperature on High-Temperature Corrosion Fracture Mechanics of Waspaloy in Various Catalyst Environments," Proceedings of High Temperature Corrosion and Protection, Materials at High Temperatures 18(2)
6. Dowson, D., "TH Hot Gas Expander Metallurgical Blade Failure Analysis", Elliott Company Report 2013.
7. Dowson, D., "Fourth Stage Steam Turbine Disk Rim Metallurgical Failure Analysis", Elliott Company Report 2013.
8. Dowson, D., "First Stage Impeller Metallurgical Failure Analysis", Elliott Company Report 2017.

ACKNOWLEDGEMENTS

The author is grateful for the support from technical services department at Elliott Group and recognizes Elliott Group for permission to publish this paper